JOURNAL OF THE KOREAN ASTRONOMICAL SOCIETY
35: 67 ~ 73, 2002

SIMULATION OF COSMIC MICROWAVE BACKGROUND POLARIZATION FIELDS FOR AMiBA EXPERIMENT

CHAN-GYUNG PARK AND CHANGBOM PARK
Astronomy Program, School of Earth and Environmental Sciences, Seoul National University, 151-742, Korea
E-mail: parkc@astro.snu.ac.kr, cbp@astro.snu.ac.kr
(Received Mar. 18, 2002; Accepted April 12, 2002)

ABSTRACT

We have made a topological study of cosmic microwave background (CMB) polarization maps by simulating the AMiBA experiment results. A ΛCDM CMB sky is adopted to make mock interferometric observations designed for the AMiBA experiment. CMB polarization fields are reconstructed from the AMiBA mock visibility data using the maximum entropy method. We have also considered effects of Galactic foregrounds on the CMB polarization fields. The genus statistic is calculated from the simulated Q and U polarization maps, where Q and U are Stokes parameters. Our study shows that the Galactic foreground emission, even at low Galactic latitude, is expected to have small effects on the CMB polarization field. Increasing survey area and integration time is essential to detect non-Gaussian signals of cosmological origin through genus measurement.

Key words: cosmic microwave background — cosmology: theory — techniques: interferometric

I. INTRODUCTION

The cosmic microwave background (CMB) polarization can provide useful information in determining cosmological parameters that are only weakly constrained by the CMB temperature anisotropy alone, such as the epoch of reionization or the presence of tensor perturbations. The Array for Microwave Background Anisotropy (AMiBA; Lo et al. 2001), an interferometric array of 19 elements, will have full polarization capabilities in order to probe the polarization properties of the CMB. In this paper, we simulate the AMiBA polarization experiment and study the topological properties of the AMiBA mock maps through the genus statistic of Q and U Stokes parameter fields. We also investigate the effect of polarized Galactic foreground emission on the CMB polarization fields.

II. SIMULATING THE AMiBA POLARIZATION EXPERIMENT

(a) Observational Strategy

An efficient observational strategy is essential to image the CMB polarization field. Although Subrahmanyan (2001) suggests *drift scanning* that is more desirable in reducing the environmental response and the cross-talk, we adopt simple observational strategy that the co-mounted array can be rotated and shifted to the adjacent points after some data acquisition. We assume that the primary beam $A(\mathbf{x})$ of an elemental aperture with diameter 0.3 m is Gaussian, normalized to unity at the peak and with the FWHM of 44′, the bandwidth of the dual polarization receivers is 20 GHz centered at 90 GHz, and the system temperature is 75 K. When 0.3 m apertures are used, the AMiBA will be sensitive to CMB polarization over the range $700 < \ell < 2000$ with signal to noise ratio of about 4 at $\ell \sim 700$ and 2 at $\ell \sim 1150$ in 24 hours (Lo et al. 2001).

We assume that 19 elements are hexagonally close-packed on a platform, as shown in Figure 1*a*, where the distances between adjacent aperture centers are 35 cm, giving 171 baselines with the minimum spacing of 35 cm. This configuration gives a good sampling of the uv-plane, and is useful for reconstructing the CMB polarization maps from the visibility data.

In a single pointing observation, the visibilities are assumed to be measured for 2 hours at a set of $\mathbf{u}$ specified by the close-packed configuration, then the instrument is rotated by 5° about an axis through the center of the aperture plane to obtain a different set of $\mathbf{u}$ with the same baseline lengths but with different orientations. In this way the uv-plane will be well-covered, allowing for good imaging. The number of rotations are chosen to be 12 times per pointing for better sampling of the uv-plane. The uv coverage after a 24 hour observation is shown in Figure 1*b*. Figures 1*c* and 1*d* show the window function in the ℓ space and the beam pattern arising from our simulation, respectively. For large $\ell \gtrsim 60$, we can relate spherical harmonic multipole index ℓ with a baseline coordinate u by $\ell = 2\pi u$ with a good approximation.

The resolution in the $\mathbf{u}$ space is limited by the area of the sky that we have surveyed. This is equal to the size of the primary beam in a single pointing observation. We can increase the resolution of the map as well as the survey area by mosaicking several contiguous pointing observations (see White et al. 1999 for more

Corresponding Author: C.-G. Park

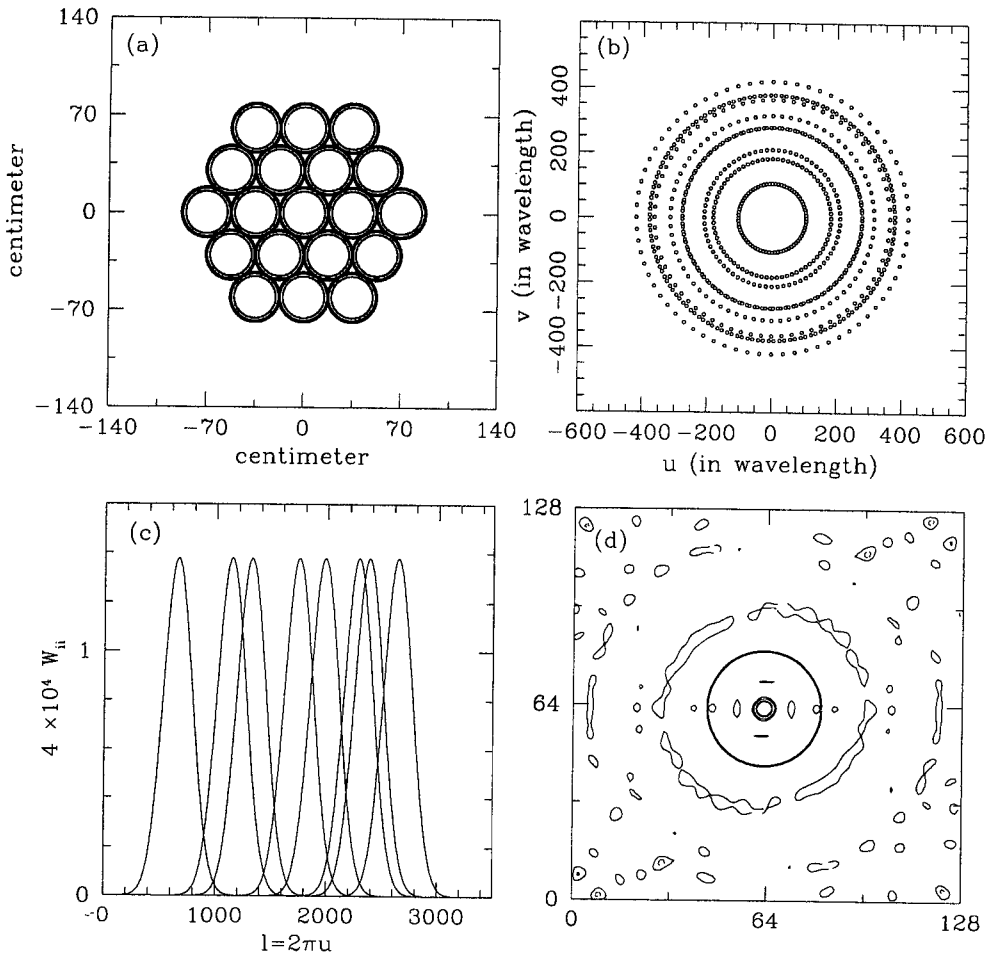

Fig. 1.— (*a*) A hexagonally close-packed configuration for AMiBA experiment, (*b*) the *uv* coverage a 24 hour observation, (*c*) the window function in the ℓ space, and (*d*) the beam pattern for a given set of *uv* coverage in a $2.^{\circ}5 \times 2.^{\circ}5$ field. A thick circle in the middle shows the FWHM (44′) of the primary beam $A(\mathbf{x})$.

details). Mosaicking does not increase the range of $\mathbf{u}$. It simply enhances our resolution by allowing us to follow more periods of a given wave, which is analogous to the Fraunhofer diffraction through many holes. In our simulated observation, we perform a mosaic survey of 9×9 pointings with spacing FWHM/2.

(b) Simulated Observations

The visibility function sampled at a pointing position $\mathbf{x}_p$ on the sky is the Fourier transform of the true sky brightness $I(\mathbf{x})$ weighted by the primary beam $A(\mathbf{x} - \mathbf{x}_p)$, i.e.,

$$V(\mathbf{u}, \mathbf{x}_p) = \int A(\mathbf{x} - \mathbf{x}_p) I(\mathbf{x}) e^{i2\pi \mathbf{u}\cdot\mathbf{x}} d^2\mathbf{x} \qquad (1)$$

(see, e.g., Ng 2001; Hobson, Lasenby, & Jones 1995). The size of the primary beam $A(\mathbf{x})$ determines the area of the sky that is viewed and hence the size of the map, while the maximum spacing determines the resolution.

In order to simulate an observation of CMB polarization fields, we follow the prescription given in Seljak (1997) and Zaldarriaga & Seljak (1997). We use the CMBFAST package (Seljak & Zaldarriaga 1996; Zaldarriaga, Seljak, & Bertschinger 1998) to get the polarization power spectrum (C_ℓ^E) and the cross-correlation between temperature and polarization (C_ℓ^C) in a flat ΛCDM model with $\Omega_\Lambda = 0.6$, $\Omega_0 = 0.4$, $h = 0.6$, and $\Omega_b h^2 = 0.0125$ (Ratra et al. 1997) in which only the E-mode (scalar mode) polarization exists and the B-mode vanishes. To generate small patches of Stokes parameter Q and U fields ($5^{\circ} \times 5^{\circ}$) on the sky we use

small-scale limit approximation by Zaldarriaga & Seljak (1997)

$$Q(\mathbf{x}) = \int d^2\mathbf{u}[E(\mathbf{u})\cos 2\phi_{\mathbf{u}} - B(\mathbf{u})\sin 2\phi_{\mathbf{u}}]e^{-i2\pi\mathbf{u}\cdot\mathbf{x}},$$

$$U(\mathbf{x}) = \int d^2\mathbf{u}[E(\mathbf{u})\sin 2\phi_{\mathbf{u}} + B(\mathbf{u})\cos 2\phi_{\mathbf{u}}]e^{-i2\pi\mathbf{u}\cdot\mathbf{x}}, \quad (2)$$

where $E(\mathbf{u})$ is the Fourier component in $\mathbf{u}$ space of E-polarization field, $\phi_{\mathbf{u}}$ is the direction angle of the two-dimensional vector $\mathbf{u}$, and $B(\mathbf{u}) = 0$. Figure 2*a* shows a realization of a pure CMB Q field in the ΛCDM model in a $5^\circ \times 5^\circ$ patch on the sky.

According to equation (1), these fields are then multiplied by the primary beam and Fourier transformed to give a regular array of visibilities. An AMiBA observation is simulated by sampling the regular array at the required points in the uv-plane specified by the AMiBA observational strategy (see Fig. 1*b*).

The AMiBA instrument noise on the data is simulated by adding a random complex number to each visibility whose the real and imaginary parts are drawn from a Gaussian distribution with the variance of the noise predicted in a real observation. Here we use the sensitivity per baseline per polarization defined as (Wrobel & Walker 1999; Ng 2001)

$$s_b = \frac{1}{\eta_s\eta_a}\frac{2k_BT_{sys}}{A_{phys}}\frac{1}{\sqrt{2\Delta\nu\tau_{acc}}}, \quad (3)$$

where $\Delta\nu$ is bandwidth, τ_{acc} is the correlator accumulation time, A_{phys} is the physical area of an elemental aperture, and η_s (η_a) is system (aperture) efficiency. Figure 2*b* shows a dirty image directly FFTed from the single pointing mock visibility data. Since the dirty image contains biased field information, it cannot be used for topology analyses. Thus we need to reconstruct the original and unbiased CMB field from the observed noisy visibility data.

(c) Image Reconstruction Using the Maximum Entropy Method

From the mock visibility data, CMB polarization fields can be reconstructed using the maximum entropy method (MEM), in which an extended emission field can be more effectively restored compared to the common CLEAN algorithm (see Narayan & Nityananda 1986 for a review, and see Conwell & Evans 1985; Chae & Yun 1994 for applications). The MEM is also more appropriate for reconstructing a non-Gaussian field, compared to the Wiener-filtering method (see, e.g., Maisinger et al. 1998). We use the methods of Cornwell & Evans (1985) for general the MEM algorithm, and of Cornwell (1988) for MEM mosaicking. However, the standard MEM method contains a logarithmic term that is inapplicable to images that have both positive and negative values, such as fluctuations in the CMB. Therefore, we consider the image to be the difference between two positive additive distributions, namely $h_i = f_i - g_i$, and the entropy becomes

$$S(\boldsymbol{h}, \boldsymbol{m}) = \sum_i \left[\psi_i - 2m_i - h_i \ln\left(\frac{\psi_i + h_i}{2m_i}\right)\right], \quad (4)$$

where h_i is the predicted map, m_i is the default model map (Maisinger, Hobson, & Lasenby 1997; Jones et al. 1998), and $\psi_i = [h_i^2 + 4m_i^2]^{1/2}$.

The attraction of MEM is that it defines the best image as the solution of a simple optimization problem obtained by maximizing the entropy while fitting to the data. Thus extra information can simply be added as constraints in the optimization. In our application of mosaicking, χ^2 is defined as

$$\chi^2 = \sum_p \sum_r \frac{|V(\mathbf{u}_r, \mathbf{x}_p) - \hat{V}(\mathbf{u}_r, \mathbf{x}_p)|^2}{\sigma^2_{V,r,p}}. \quad (5)$$

Here $\hat{V}$ denotes the predicted visibility, and $\sigma^2_{V,r,p}$ is the variance in the visibility of the rth visibility sample at the pth pointing (see Cornwell 1988 for more details).

Maximizing

$$J \equiv S - \alpha\chi^2, \quad (6)$$

where α is a Lagrange multiplier, gives a solution for $\boldsymbol{h}$ that maximizes the entropy and fits to the data. We find the most appropriate image iteratively using the Newton-Raphson method, i.e.,

$$\Delta\boldsymbol{h} = (-\nabla\nabla J)^{-1} \cdot \nabla J. \quad (7)$$

Here we choose the default model map as $\boldsymbol{m} = 5\ \mu$K, constant everywhere, and the Lagrange multiplier as $\alpha = 100$. These values are insensitive to the final solution. The mosaicked images reconstructed by MEM are very close to the original CMB polarization maps (compare Fig. 2*c* with Fig. 2*a*). Figure 3 compares the CMB Q and U fields along a row in the original map (dotted curves) with those in the MEM map reconstructed from 9×9 mosaic data (solid curves).

(d) Galactic Foregrounds

We investigate the effects of polarized Galactic foreground emission on the CMB polarization fields. Two possible sources of the polarized Galactic emission are synchrotron and spinning dust emissions, which are known to induce at least 10 % polarization fraction at frequencies below 90 GHz (Lubin & Smoot 1981). Vibrational dust and free-free emissions are expected to be unpolarized. We use a simple toy model of Kogut & Hinshaw (2000) to make foreground polarization maps. We assume here that mean fractional polarization is 10 %, the polarized Galactic emission is proportional to the unpolarized intensity, and the effect of synchrotron emission is negligible at 90 GHz. We can model the Stokes Q and U components as

$$Q = f\cos(2\gamma)I, \quad U = f\sin(2\gamma)I, \quad (8)$$

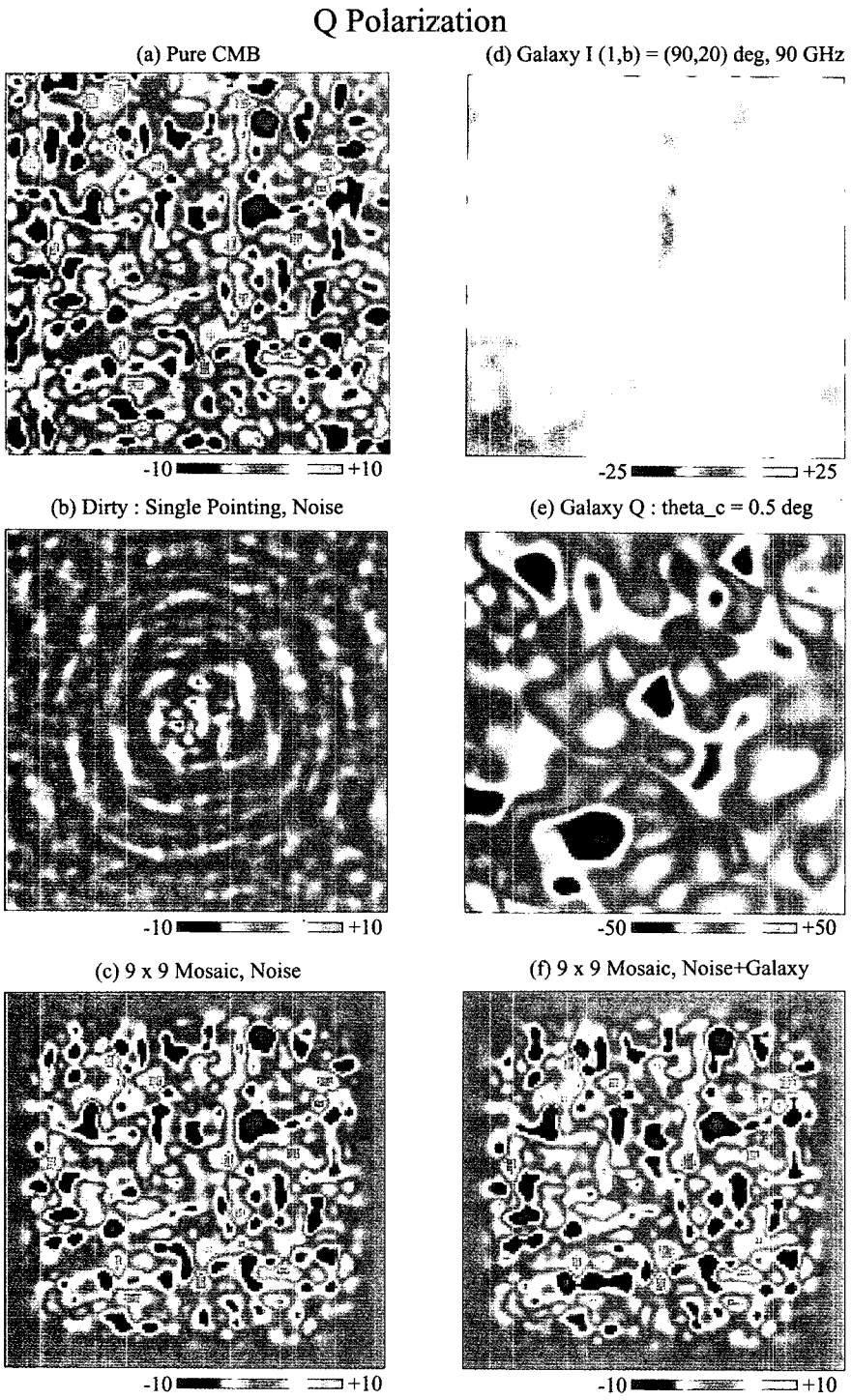

Fig. 2.— Examples of mock CMB Q polarization fields, Galactic foregrounds, and MEM reconstructed fields. All numbers given in colorbars have a unit of μK.

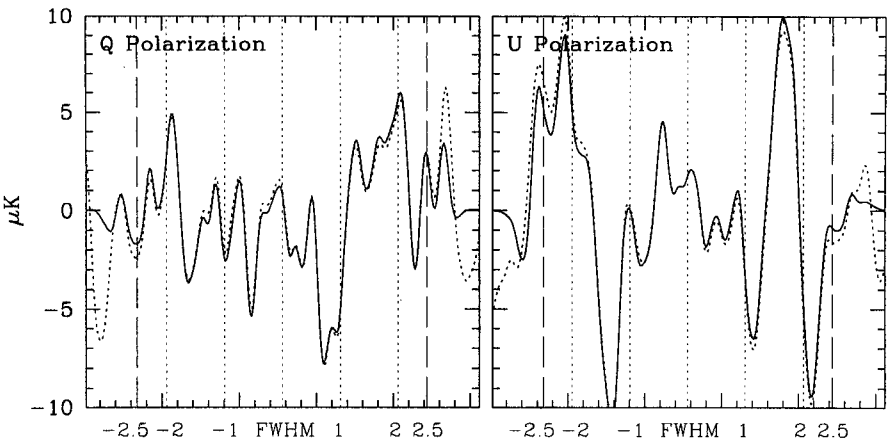

Fig. 3.— Profiles of the CMB Q and U fields along a row in the original maps (dotted curves) and in the MEM reconstructed maps (solid curves).

where $f(\boldsymbol{\theta})$ is the fractional polarization, assumed to vary across the sky with $\langle f \rangle = 0.1$, and $\gamma(\boldsymbol{\theta})$ is the polarization angle which is randomly realized with coherence angle $\theta_c = 0.^\circ 5$ (see §2 of Kogut & Hinshaw 2000 for more details). We use a two-component dust model of Finkbeiner, Davis, & Schlegel (1998) to predict 90 GHz vibrational dust intensity, and a model of Kogut et al. (1996) for adding the free-free emission. The 100 μm dust map of Schlegel, Finkbeiner, & Davis (1998) is used as a basic template map. Figures 2*d*, 2*e*, and 2*f* show the 90 GHz Galactic intensity at $b = 20°$, its Q polarized contribution, and the MEM reconstructed CMB Q polarized field contaminated by the Galactic polarized foreground, respectively.

III. TOPOLOGY OF THE SIMULATED MAPS

The CMB polarization field, like the temperature anisotropy, can be used for an observational test of the Gaussianity of the primordial density fluctuation, and thus provide an important constraint on the inflationary models. We use the two-dimensional genus statistic introduced by Gott et al. (1990) as a quantitative measure for the topology of the CMB polarization fields. The genus is defined as the number of hot spots minus the number of cold spots, or equivalently,

$$g(\nu) = \frac{1}{2\pi} \int_C \kappa ds, \tag{9}$$

where κ is the signed curvature of the iso-temperature contours C. Since the genus curve as a function of the temperature threshold level has a form of $g(\nu) \propto \nu e^{-\nu^2/2}$ for a Gaussian random-phase field, non-Gaussianity of a field can be detected from deviations of the genus curve from this relation. For example, non-Gaussianity can cause shift or asymmetry of the genus curve.

We present genus curves as a function of the area-fraction threshold level ν_A, which is defined to be the temperature threshold level at which the corresponding iso-temperature contours enclose a fraction of the survey area equal to that of a Gaussian field (Gott et al. 1990). All measured values are averages over 15 mock AMiBA surveys. We use the 4 FWHM × 4 FWHM region in each mock survey field, where the MEM reconstruction gives more confident results. Figures 4*a* and 4*b* shows averaged histograms and genus for foreground-free (solid curve), Galactic foreground-added (open circles), and Galactic foreground-added and MEM reconstructed (9 × 9 mosaic observation, filled circles) CMB Q fields. The last case is a result of a 24 hour integration per pointing located at Galactic latitude $b = 20°$. Note that the solid curve in Figure 4*b* shows the functional form expected for a random-phase Gaussian field, $A\nu e^{-\nu^2/2}$, and has been fitted to the foreground-free genus result by adjusting A. The result from a 24 hour integration of a region centered at $b = 35°$ is shown in Figure 4*c*. When the integration time is only one hour per pointing, we obtain genus curves shown in Figure 4*d*.

Table 1 lists skewness $\langle (Q/\sigma)^3 \rangle$, genus-related statistics A (amplitude), $\Delta\nu$ (shift parameter), and Δg (asymmetry parameter) measured from CMB Q fields; see Peebles (1993) for skewness and Park et al. (2001) for definition and measurement of genus-related statistics, respectively.

The results show that the polarized Galactic emissions, even at low latitude, do not have significant effect on the CMB polarization fields. Although the polarized Galactic foreground emissions at $b = 20°$ cause slight asymmetry, and reduce genus amplitude (Fig. 4*b* and Table 1), these effects are smaller than the statistical fluctuations due to the sample variance of the pure CMB map. The open and filled circles in each panel in Figure 4 show that the original polarization fields can be well restored from the AMiBA mosaic observational data by MEM image reconstruction technique if the integration time is 24 hours per pointing. However,

Table 1. Skewness and Genus Statistics Measured from Mock CMB Q Fields

	Q Pol.	$\langle(Q/\sigma)^3\rangle$	A	$\Delta\nu$	Δg
	CMB	-0.08 ± 0.11	52.5 ± 4.4	-0.006 ± 0.035	0.04 ± 0.10
$b = 20°$	+Galaxy	-0.06 ± 0.16	47.9 ± 4.7	-0.005 ± 0.047	0.04 ± 0.12
	+Galaxy (observed)†	-0.05 ± 0.15	48.6 ± 4.6	-0.014 ± 0.044	0.03 ± 0.12
$b = 35°$	+Galaxy	-0.07 ± 0.13	51.6 ± 3.9	-0.009 ± 0.040	0.05 ± 0.11
	+Galaxy (observed)†	-0.06 ± 0.12	52.9 ± 4.2	-0.008 ± 0.037	0.02 ± 0.09

† 9 × 9 mosaic observation with 24 hours integration time per pointing.

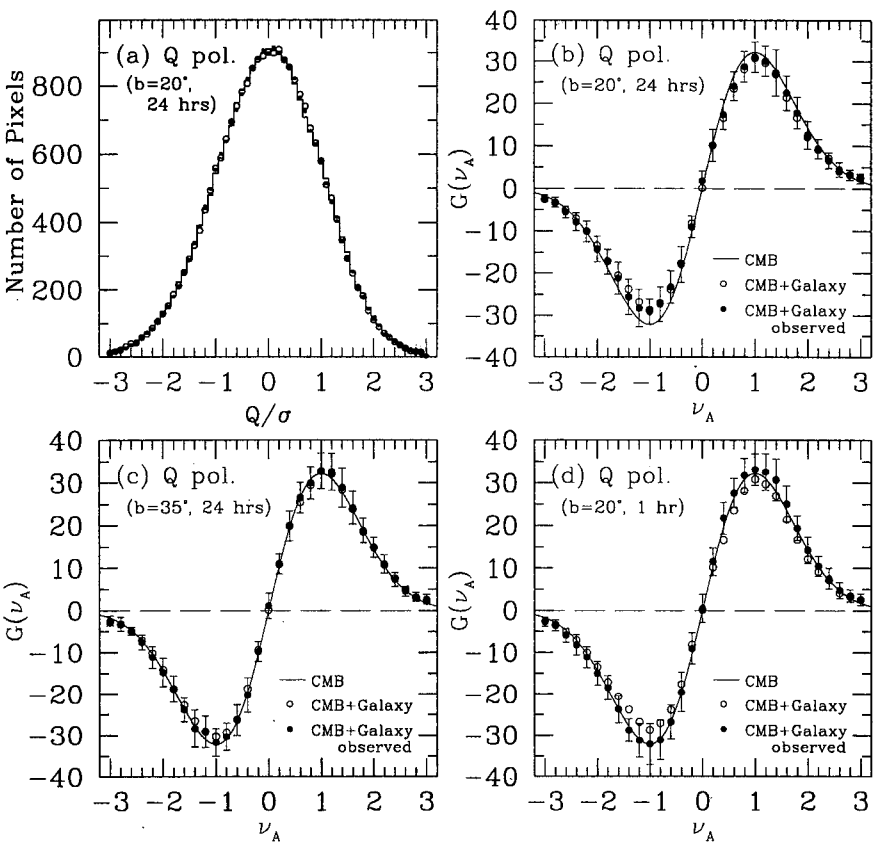

Fig. 4.— Histograms and genus measured from CMB polarization Q maps.

if the integration time is one hour, instrumental noise increases the amplitude of the genus curve, and the presence of non-Gaussian signals due to the Galactic emission is buried.

IV. CONCLUSIONS

We have studied the topology of CMB polarization maps by simulating the AMiBA experiment and by measuring the skewness and genus statistics. The MEM turns out to be very useful in reconstructing the CMB polarization Q and U fields from the interferometric visibility data. Our study shows that although the polarized Galactic foreground emissions at low latitude ($b = 20°$) decrease the amplitude of the genus curve and cause asymmetry of the curve, these effects are not significant compared with the sample variance in our $2.^{\circ}9 \times 2.^{\circ}9$ surveys. At higher Galactic latitudes, the effects of the Galactic emissions i s shown to be negligible, and the intrinsic non-Gaussianity of the CMB polarization is easier to detect.

The major source of statistical variance of the genus statistic is the sample variance induced by our small survey area (4 FWHM × 4 FWHM = 8.6 deg.^{2}). This can be reduced not by observing many small different patches of the sky, but by increasing the area of the survey at each location. Therefore, increasing the survey area and integration time at a given pointing is essential to accurately estimate the effects of Galactic foregrounds on the polarization maps and to detect non-Gaussian signals of cosmological origin.

We acknowledge valuable discussions with Kin-Wang

Ng, Uros Seljak and Ravi Subrahmanyan. This work is supported by the BK21 program of the Korean Government.

REFERENCES

Chae, J.-C., & Yun, H.S. 1994, Maximum power entropy method for low contrast images, JKAS, 27, 191

Cornwell, T.J. 1988, Radio-interferometric imaging of very large objects, A&A, 202, 316,

Cornwell, T.J., & Evans, K.F. 1985, A simple maximum entropy deconvolution algorithm, A&A, 143, 77

Finkbeiner, D.P., Davis, M., & Schlegel, D.J. 1999, Extrapolation of Galactic dust emission at 100 microns to cosmic microwave background radiation frequencies using FIRAS, ApJ, 524, 867

Gott, J.R., Park, C., Juszkiewicz, R., Bies, W.E., Bennett, D.P., Bouchet, F.R., & Stebbins, A. 1990, Topology of microwave background fluctuations – Theory, ApJ, 352, 1

Hobson, M.P., Lasenby, A.N., & Jones, M. 1995, A Bayesian method for analysing interferometer observations of cosmic microwave background fluctuations, MNRAS, 275, 863

Jones, A.W. et al. 1998, 10-GHz Tenerife cosmic microwave background observations at 8 deg resolution and their analysis using a new maximum entropy method, MNRAS, 294, 582

Kogut, A., Banday, A.J., Bennett, C.L., Górski, K.M., Hinshaw, G., Smoot, G.F., & Wright, E.L. 1996, Microwave emission at high Galactic latitude in the four-year DMR sky maps, ApJ, 464, L5

Kogut, A., & Hinshaw, G. 2000, Simulations of foreground effects for cosmic microwave background polarization, ApJ, 543, 530

Lo, K.Y., Chiueh, T.H., Martin, R.N., Ng, K.-W., Liang, H., Pen, U.-L., & Ma, C.-P. 2001, AMiBA: Array for Microwave Background Anisotropy, in New Cosmological Data and the Values of the Fundamental Parameters, IAU Symp. 201, ed. A. Lasenby & A. Wilkinson (Astronomical Society of the Pacific, San Francisco, CA, 2001)

Maisinger, K., Hobson, M.P., & Lasenby, A.N. 1997, A maximum entropy method for reconstructing interferometer maps of fluctuations in the cosmic microwave background radiation, MNRAS, 290, 313

Maisinger, K., Hobson, M.P., Lasenby, A.N., & Turok, N. 1998, The observability of topological defects with ground-based interferometers, MNRAS, 297, 531

Narayan, R., & Nityananda, R. 1986, Maximum entropy image restoration in astronomy, ARA&A, 24, 127

Ng, K.-W. 2001, Complex visibilities of cosmic microwave background anisotropies, Phys. Rev. D, 63, 123001

Park, C.-G., Park, C., Ratra, B., & Tegmark, M. 2001, Gaussianity of degree-scale cosmic microwave background anisotropy observations, ApJ, 556, 582

Peebles, P.J.E. 1993, Principles of Physical Cosmology, (Princeton University Press, Princeton, New Jersey), Chapter 19

Ratra, B., Sugiyama, N., Banday, A.J., & Górski, K.M. 1997, Cosmic microwave background anisotropy in COBE DMR-normalized open and flat-Λ cold dark matter cosmogonies, ApJ, 481, 22

Schlegel, D.J., Finkbeiner, D.P., & Davis, M. 1998, Maps of dust infrared emission for use in estimation of reddening and cosmic microwave background radiation foregrounds, ApJ, 500, 525

Seljak, U. 1997, Measuring polarization in the cosmic microwave background, ApJ, 482, 6

Seljak, U., & Zaldarriaga, M. 1996, A line-of-sight integration approach to cosmic microwave background anisotropies, ApJ, 469, 437

Subrahmanyan, R. 2002, Observing the CMB with the AMiBA, in AMiBA 2001: High-Z Clusters, Missing Baryons, and CMB Polarization, ed. L.W. Chen, C.-P. Ma, K.-W. Ng, and U.-L. Pen, ASP Conference Series Vol. 257 (Astronomical Society of the Pacific, San Fransisco, CA, 2002)

White, M., Carlstrom, J.E., Dragovan, M., & Holzapfel, W.L. 1999, Interferometric observation of cosmic microwave background anisotropies, ApJ, 514, 12

Wrobel, J.M., & Walker, R.C. 1999, Sensitivity, in Synthesis Imaging in Radio Astronomy II, ed. G.B. Taylor, C.L. Carilli, and R.A. Perley, ASP Conference Series Vol. 180 (Astronomical Society of the Pacific, San Fransisco, CA, 1999)

Zaldarriaga, M., & Seljak, U. 1997, All-sky analysis of polarization in the microwave background, Phys. Rev. D, 55, 1830

Zaldarriaga, M., Seljak, U., & Bertschinger, E. 1998, Integral solution for the microwave background anisotropies in nonflat universes, ApJ, 494, 491